Aalborg Universitet

Control and Modeling of Push-Pull Forward Three-Level Converter for Microgrid

Yao, Zhilei; Xu, Jing; Guerrero, Josep M.

Control and Modeling of Push-Pull Forward Three-Level Converter for Microgrid

Zhilei Yao
Research Institute of Jiangsu Coastal
Renewable Energy Vehicle
Yancheng Institute of Technology
Yancheng 224051, P. R. China
Email: nhyzl@163.com

Jing Xu
School of Information Engineering
Yancheng Institute of Technology
Yancheng 224051, P. R. China
Email: xujingycit@163.com

Josep M. Guerrero
Department of Energy Technology
Aalborg University
Aalborg 9220, Denmark
Email: joz@et.aau.dk

Abstract—Renewable energy sources are widely used in microgrid. Output voltage of them is often low and varies widely. Because diodes in three-level legs in traditional three-level (TL) converter are substituted by MOSFETs, the push-pull forward (PPF) TL converter is very suitable for wide and low input-voltage applications. It can operate at two-level and three-level modes. Modeling of the proposed converter is established. Control of the proposed converter is designed, which contains output voltage loop and current limit loop. In addition, control block diagrams of both modes can be simplified to one control diagram. By adding input voltage feedforward, influences of input voltage on output voltage and inductor current can be eliminated. The divider in the input voltage feedforward is simplified by two piecewise linear functions, which can be easily implemented by operational amplifiers. Therefore, cost can be reduced. Simulation results of a 1-kW PPF TL converter verify the theoretical analysis.

Keywords—three-level converter; DC-DC converter; three-level mode; two-level mode; input voltage feedforward

I. INTRODUCTION

Microgrids support a flexible and efficient electric grid, powered by renewable energy sources, such as fuel cell and PV cell [1]. However, output voltage of renewable energy sources is often low and wide range, such as 20-50 V [2]. The three-level (TL) converter is very suitable for wide input-voltage range application, which can reduce the filter inductor current ripple and solve the problem of high voltage stress of the output rectifier diodes in conventional two-level voltage-source converter [3]-[4]. Nevertheless, conduction loss of the diodes in three-level legs in the traditional TL converter is high in low input-voltage application.

A push-pull forward (PPF) TL converter for low and wide input-voltage range application was proposed in [5]. The freewheeling diodes connected with three-level legs are substituted for the MOSFETs to reduce the conduction loss, so one more control degree of freedom is added compared with the conventional TL converter. Only operating principle is illustrated in [5].

The TL converter for wide input-voltage range application can operate at three-level and two-level modes, two control degrees of freedom exist [6]-[7]. However, modeling of the TL converter is not given. Moreover, three control degrees of freedom exist in the PPF TL converter, so it is necessary to establish modeling of the PPF TL converter and simplify the control at three-level and two-level modes.

In addition, input voltage feedforward is often added to the control system in order to eliminate influences of input voltage on output voltage and output filter inductor current in wide input-voltage range application [8]-[10]. Since the function of the input voltage feedforward is inversely proportional to the input voltage [9], it is complicated to implement. For example, a divider is often needed [10]. Therefore, cost is increased. A linear function of the input voltage is used in [9]. However, the error between the ideal feedforward signal and the linear function is large.

In order to solve the aforementioned problems, control and modeling of the PPF TL converter is proposed. The operating principle is illustrated in Section II. Only two independent control variables are needed, which are the same as the traditional TL converter. Then modeling of the PPF TL converter is established in Section III. Small-signal model of the PPF TL converter is deduced. Section IV gives the control design and example for the PPF TL converter. Output voltage controller, current limit regulator, and input voltage feedforward are designed in detail. Simulation results of a 1-kW PPF TL converter verify the theoretical analysis in Section V. Finally, the concluding remarks are given in Section VI.

II. OPERATING PRINCIPLE

Fig. 1 shows the PPF TL converter, where R_{ESR} is the equivalent series resistance of filter capacitor (C_f), i_L is the current through output filter inductor (L_f), R_L is the load, and $D_{S1} \sim D_{S6}$ are the body diodes of switches $S_1 \sim S_6$, respectively. Fig. 2 gives key waveforms of the proposed converter, where t_{on1} is turn-on time of S_1 or S_4, t_{on2} is turn-on time of S_2 or S_3, T_s is the switching period, and n is the windings ratio of secondary and primary windings. There are two methods to control S_5 and S_6. On the one hand, S_1 and S_5 can be complementary switched; S_4 and S_6 can be turned complementary, as shown in Fig. 2. S_2 and S_3 only sustain input voltage (U_{in}) in two-level mode. On the other hand, the drive signal of S_5 is that of S_2 ANDing with NOT that of S_1. Likewise, the drive signal of S_6 is that of S_3 ANDing with NOT that of S_4. S_2 and S_3 sustain one and one-half of U_{in} in two-level mode. Therefore, the former control method is

selected to reduce the voltage stresses of S_2 and S_3. Detailed operating principle can be referred to [5].
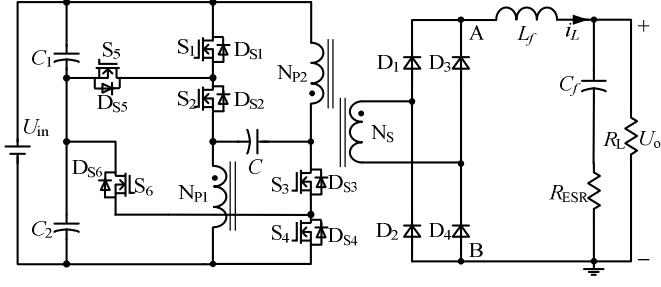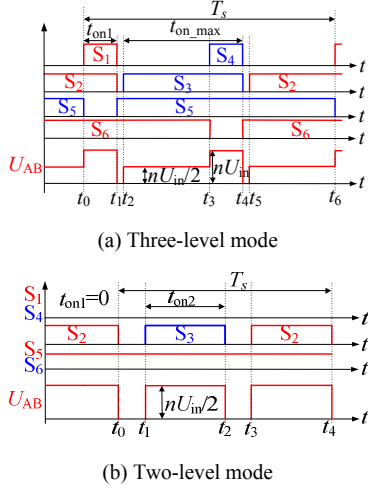

Fig. 1. Main circuit of the PPF TL converter.

(a) Three-level mode

(b) Two-level mode

Fig. 2. Key waveforms of the PPF TL converter.

In three-level mode, S_1 and S_4 are PWM controlled. S_2 and S_3 are switched out of phase with a small dead time, so t_{on2} is equal to the maximum turn-on time (t_{on_max}), which is constant. The secondary rectified voltage ($\bar{U}_{AB}$) is a three-level waveform. In two-level mode, S_2 and S_3 are PWM controlled. S_1 and S_4 are turned off all the time, whereas S_5 and S_6 are always turned on in this mode. Voltage U_{AB} is a two-level waveform.

From above analysis and Fig. 2, there are only two independent control variables in the proposed converter, which are the same as that in traditional TL converters.

III. MODELING OF THE PPF TL CONVERTER

From Figs. 1 and 2, there are three types of levels of U_{AB}, i.e., 0 level, 1/2 level, and 1 level, shown in Fig. 3. The state-space equations of 0 level, 1/2 level, and 1 level are given in (1), (2), and (3), respectively.
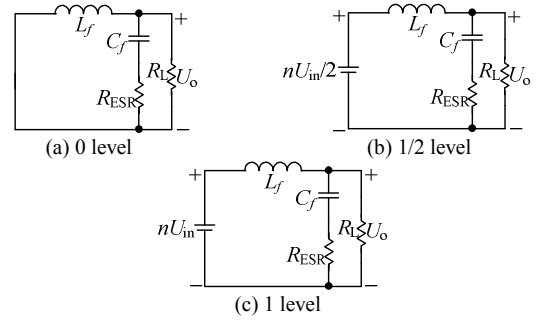

(a) 0 level   (b) 1/2 level

(c) 1 level

Fig. 3. Different types of equivalent circuits.

The average state-space equation can be deduced from (1)-(3), as shown in (4), where u_{cf} is the voltage across C_f, d_1 is the duty ratio of S_1 that is t_{on1}/T_s and d_2 is the duty cycle of S_2, i.e., t_{on2}/T_s.

$$\begin{pmatrix} \dot{i}_L \\ \dot{u}_{cf} \end{pmatrix} = \begin{pmatrix} -\dfrac{R_L R_{ESR}}{L_f(R_L + R_{ESR})} & -\dfrac{R_L}{L_f(R_L + R_{ESR})} \\ \dfrac{R_L}{C_f(R_L + R_{ESR})} & \dfrac{-1}{C_f(R_L + R_{ESR})} \end{pmatrix} \begin{pmatrix} i_L \\ u_{cf} \end{pmatrix} \tag{1}$$

$$\begin{pmatrix} \dot{i}_L \\ \dot{u}_{cf} \end{pmatrix} = \begin{pmatrix} -\dfrac{R_L R_{ESR}}{L_f(R_L + R_{ESR})} & -\dfrac{R_L}{L_f(R_L + R_{ESR})} \\ \dfrac{R_L}{C_f(R_L + R_{ESR})} & \dfrac{-1}{C_f(R_L + R_{ESR})} \end{pmatrix} \begin{pmatrix} i_L \\ u_{cf} \end{pmatrix} + \begin{pmatrix} \dfrac{n}{2L_f} \\ 0 \end{pmatrix} U_{in} \tag{2}$$

$$\begin{pmatrix} \dot{i}_L \\ \dot{u}_{cf} \end{pmatrix} = \begin{pmatrix} -\dfrac{R_L R_{ESR}}{L_f(R_L + R_{ESR})} & -\dfrac{R_L}{L_f(R_L + R_{ESR})} \\ \dfrac{R_L}{C_f(R_L + R_{ESR})} & \dfrac{-1}{C_f(R_L + R_{ESR})} \end{pmatrix} \begin{pmatrix} i_L \\ u_{cf} \end{pmatrix} + \begin{pmatrix} \dfrac{n}{L_f} \\ 0 \end{pmatrix} U_{in} \tag{3}$$

$$\begin{pmatrix} \dot{i}_L \\ \dot{u}_{cf} \end{pmatrix} = \begin{pmatrix} -\dfrac{R_L R_{ESR}}{L_f(R_L + R_{ESR})} & -\dfrac{R_L}{L_f(R_L + R_{ESR})} \\ \dfrac{R_L}{C_f(R_L + R_{ESR})} & \dfrac{-1}{C_f(R_L + R_{ESR})} \end{pmatrix} \begin{pmatrix} i_L \\ u_{cf} \end{pmatrix} + \begin{pmatrix} \dfrac{n(d_1 + d_2)}{L_f} \\ 0 \end{pmatrix} U_{in} \tag{4}$$

$$\begin{pmatrix} \hat{i}_L \\ \hat{u}_o \end{pmatrix} = \begin{pmatrix} \dfrac{n[1+C_f(R_L+R_{ESR})s](d_1+d_2)}{N(s)} & \dfrac{n[1+C_f(R_L+R_{ESR})s]U_{in}}{N(s)} & \dfrac{n[1+C_f(R_L+R_{ESR})s]U_{in}}{N(s)} \\[4mm] \dfrac{nR_L(1+R_{ESR}C_f s)(d_1+d_2)}{N(s)} & \dfrac{nR_L(1+R_{ESR}C_f s)U_{in}}{N(s)} & \dfrac{nR_L(1+R_{ESR}C_f s)U_{in}}{N(s)} \end{pmatrix} \begin{pmatrix} \hat{u}_{in} \\ \hat{d}_1 \\ \hat{d}_2 \end{pmatrix} \quad (6)$$
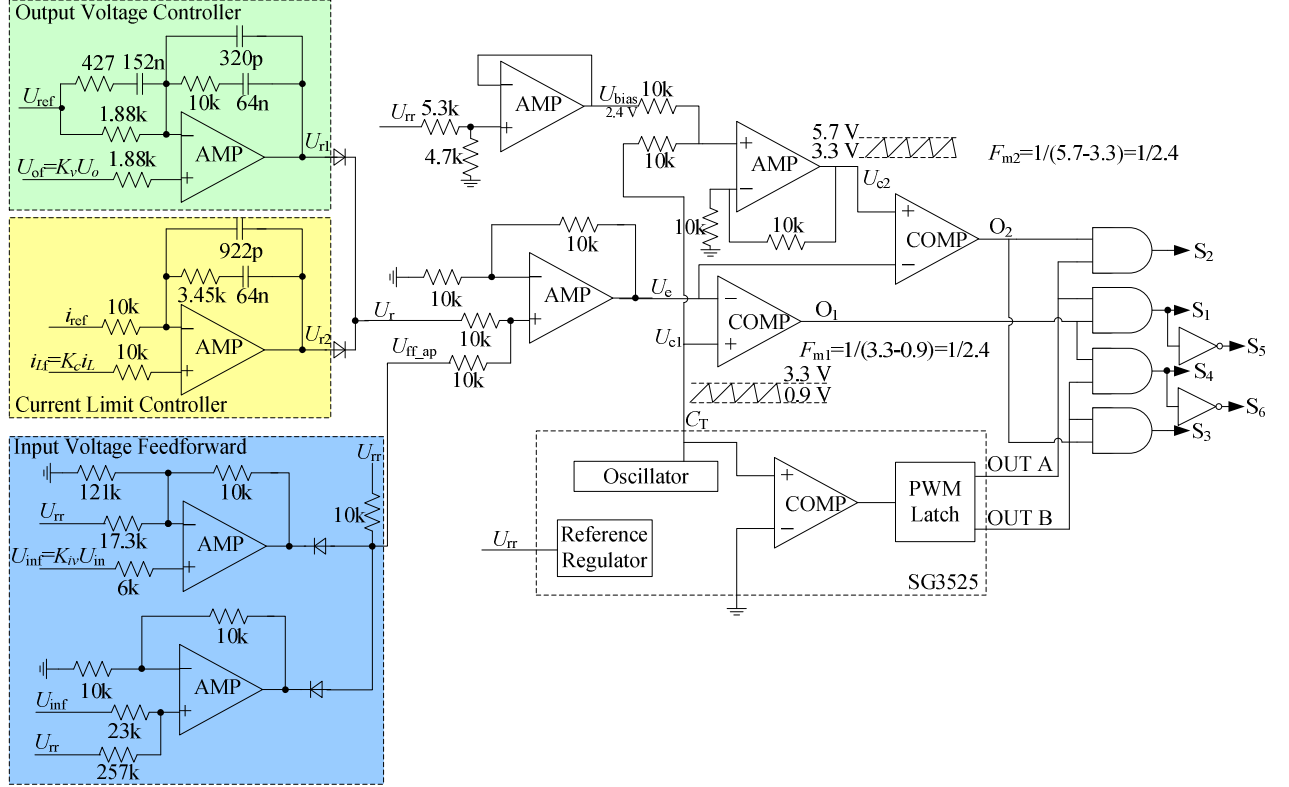

Fig. 4. Whole control system.

TABLE I.   DESIGN PARAMETERS

Input voltage (U_{in})	20-50 V
Output voltage (U_o)	380 V
Output power (P_o)	1 kW
Switching frequency (f_s)	100 kHz
Gain of the modulator (F_{m1} and F_{m2})	1/2.4
Feedback coefficient of output voltage (K_v)	5/380
Feedback coefficient of input voltage (K_{iv})	0.1
Feedback coefficient of i_L (K_c)	0.6
Secondary to primary turns ratio of the transformer (n)	20.5
Output filter capacitor (C_f)	470 μF
ESR of C_f (R_{ESR})	138 mΩ
Output filter inductor (L_f)	640 μH

Relationship between u_{cf} and output voltage u_o can be obtained from Fig. 1.

$$\dot{u}_{cf} = \frac{-1}{C_f R_{ESR}} u_{cf} + \frac{1}{C_f R_{ESR}} u_o . \quad (5)$$

From (4) and (5), small-signal model can be deduced, shown in (6) at the top of this page, where $N(s) = L_f C_f(R_{ESR}+R_L)s^2 + (R_L C_f R_{ESR} + L_f)s + R_L$.

IV. CONTROL DESIGN AND EXAMPLE

The whole control system is given in Fig. 4, where only one control chip SG3525 is used.

A. Specifications

The parameters used in the control design are shown in Table I.

B. Output Voltage Controller

As seen from Section II, in three-level mode, only d_1 is regulated, while d_2 is equal to d_{max}, i.e., t_{on_max}/T_s. In two-level mode, only d_2 is regulated, whereas d_1 equals to 0. Therefore, only one variable (d_1 or d_2) is controlled in each mode. In addition, the transfer functions of both duty ratios to output voltage are the same, i.e., $G_{vd1}(s) = G_{vd2}(s) = G_{vd}(s)$. Thus, control block diagrams of output voltage loop is shown in Fig. 5, where $G_{vr}(s)$ is the transfer function of output voltage regulator, and F_{m1} and F_{m2} are gains of the modulators in three-level and two-level modes, respectively.

$$G_{vd}(s) = \frac{\hat{u}_o}{\hat{d}} = \frac{nR_L(1+R_{ESR}C_f s)U_{in}}{L_f C_f(R_{ESR}+R_L)s^2 + (R_L C_f R_{ESR} + L_f)s + R_L} \quad (7)$$
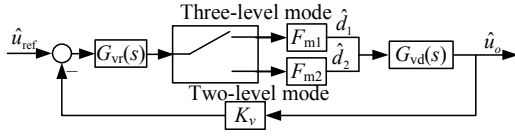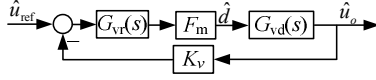
Fig. 5. Control block diagram of the output voltage loop.

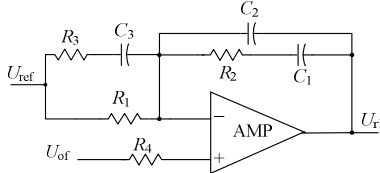Fig. 6. Simplified control block diagram of the output voltage loop.

Fig. 7. Output voltage controller.

If F_{m1} and F_{m2} are set to the same, i.e., F_m, by adjusting the amplitude of the carrier waveforms, control block diagram in both modes can be simplified to Fig. 6. Therefore, performance of the system at both three-level and two-level modes is the same by using the same controller. In addition, control design of the system can be simplified.

From Fig. 6 and (7), the open loop transfer function under voltage controlled mode can be obtained as

$$G_v(s) = G_{vd}(s) \times F_m \times K_v$$
$$= \frac{nR_L(1+R_{ESR}C_f s)U_{in}}{L_f C_f (R_{ESR} + R_L)s^2 + (R_L C_f R_{ESR} + L_f)s + R_L} \times \frac{1}{2.4} \times \frac{5}{380}. \quad (8)$$

The crossover frequency is set to 5 kHz at $U_{in} = 50$ V. From (8), about a zero of 2.5 kHz is generated by C_f and R_{ESR}, which is close to the crossover frequency during the whole input-voltage range. Therefore, a type III compensation network is adopted to eliminate the zero, as shown in Fig. 7, where U_{r1} is the output of voltage regulator. The transfer function of the controller is given in (9).

$$G_{vr}(s) = \frac{(1 + R_2 C_1 s)[1 + s(R_1 + R_3)C_3]}{sR_1(C_1 + C_2)(1 + s\frac{R_2 C_1 C_2}{C_1 + C_2})(1 + sR_3 C_3)} \quad (9)$$

From (9), the following two zeros and three poles can be deduced.

$$f_{z1} = \frac{1}{2\pi R_2 C_1} \quad (10)$$

$$f_{z2} = \frac{1}{2\pi(R_1 + R_3)C_3} \quad (11)$$

$$f_{p1} = 0 \quad (12)$$

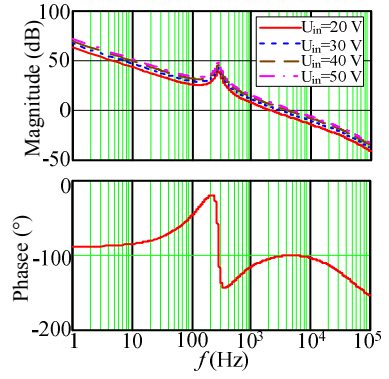$$f_{p2} = \frac{1}{2\pi R_3 C_3} \quad (13)$$

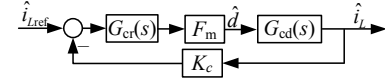Fig. 8. Bode diagram of output voltage loop.

Fig. 9. Simplified control block diagram of the current limit loop.

$$f_{p3} = \frac{1}{2\pi \frac{R_2 C_1 C_2}{C_1 + C_2}} \quad (14)$$

The zeros and poles are set as follows:

1) the zeros f_{z1} and f_{z2} are set as 250 Hz to maintain the phase margin being larger than 45°;

2) the pole f_{p2} is equal to the zero of 2.5 kHz generated by C_f and R_{ESR};

3) the pole f_{p3} is set as half of the switching frequency to attenuate high frequency noise, i.e., 50 kHz.

Therefore, parameters C_1, C_2, C_3, R_1, R_2, R_3, and R_4 can be calculated as 64 nF, 320 pF, 152 nF, 1.88 kΩ, 10 kΩ, 427 Ω, and 1.88 kΩ. In addition, the bode diagram of output voltage loop can be obtained, given in Fig. 8. From Fig. 8, the crossover frequency is between 2 kHz and 5 kHz under the input voltage range of 20-50 V. Moreover, the phase margin is between 74.47° and 78.94°.

C. Current Limit Controller

In order to limit the output filter inductor current during startup or overload, a current limit loop should be added limiting the output filter inductor current to three times the rated load current.

Since the transfer functions of both duty ratios to inductor current are also the same, i.e., $G_{cd1}(s) = G_{cd2}(s) = G_{cd}(s)$ from (6), the simplified control block diagram of the current limit loop can be obtained like output voltage loop, as shown in Fig. 9, where $G_{cr}(s)$ is the transfer function of current regulator.

$$G_{cd}(s) = \frac{\hat{i}_{L_f}}{\hat{d}} = \frac{n[1 + C_f(R_{ESR} + R_L)s]U_{in}}{L_f C_f(R_{ESR} + R_L)s^2 + (R_L C_f R_{ESR} + L_f)s + R_L} \quad (15)$$

From Fig. 9 and (15), the open loop transfer function under current limit controlled mode can be expressed as
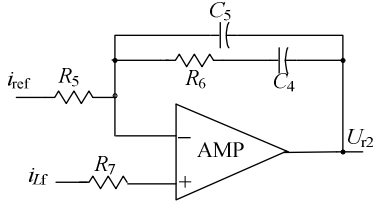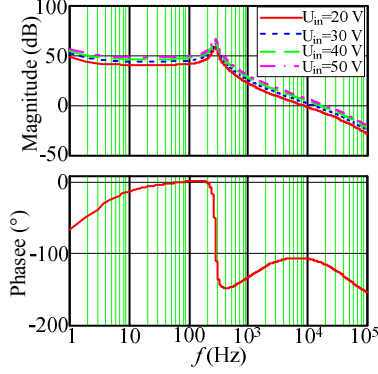
Fig. 10. Current limit controller.

Fig. 11. Bode diagram of current limit loop.

$$G_c(s) = G_{cd}(s) \times F_m \times K_c$$
$$= \frac{n[1 + C_f(R_{ESR} + R_L)s]U_{in}}{L_f C_f (R_{ESR} + R_L)s^2 + (R_L C_f R_{ESR} + L_f)s + R_L} \times \frac{0.6}{2.4} \quad (16)$$

The crossover frequency is set to 20 kHz at $U_{in} = 50$ V. From (16), about a zero of 2.5 Hz is generated by C_f, R_L, and R_{ESR}, which can improve the phase margin of the system. Thus, a type II compensation network is used, as shown in Fig. 10, where U_{r2} is the output of current limit regulator. The transfer function of the controller is given in (17).

$$G_{cr}(s) = \frac{1 + R_6 C_4 s}{s R_5 (C_4 + C_5)(1 + s R_6 C_5)} \quad (17)$$

From (17), the following one zero and two poles can be obtained.

$$f_{z3} = \frac{1}{2\pi R_6 C_4} \quad (18)$$

$$f_{p4} = 0 \quad (19)$$

$$f_{p5} = \frac{1}{2\pi R_6 C_5} \quad (20)$$

The zero and pole are set as follows:

1) the zero f_{z3} is set as 1 kHz to maintain the phase margin being larger than $45°$;

2) the pole f_{p5} is the same as f_{p3} to attenuate high frequency noise.

Therefore, parameters C_4, C_5, R_5, R_6, and R_7 can be calculated as 64 nF, 922 pF, 10 kΩ, 3.45 kΩ, and 10 kΩ. In addition, the bode diagram of current limit loop can be obtained, given in Fig. 11. From Fig. 11, the crossover frequency is between 8.6 kHz and 20 kHz under the input voltage range of 20-50 V. Moreover, the phase margin is between $65.4°$ and $73.8°$.

D. Input Voltage Feedforward

From (6), the input-to-output voltages and input voltage-to-inductor current transfer functions can be obtained as

$$G_{oi}(s) = \frac{\hat{u}_o}{\hat{u}_{in}} = \frac{n R_L (1 + R_{ESR} C_f s)(d_1 + d_2)}{L_f C_f (R_{ESR} + R_L)s^2 + (R_L C_f R_{ESR} + L_f)s + R_L} \quad (21)$$

$$G_{ci}(s) = \frac{\hat{i}_{L_f}}{\hat{u}_{in}} = \frac{n[1 + C_f(R_L + R_{ESR})s](d_1 + d_2)}{L_f C_f (R_{ESR} + R_L)s^2 + (R_L C_f R_{ESR} + L_f)s + R_L} \quad (22)$$

As the change of input voltage affects the output voltage and inductor current from (21) and (22), respectively, input voltage feedforward should be added into the control system. The quiescent operation point of reference voltage (U_{ff_th}) should be added into the common point of the output voltage and inductor current regulators, given in (23).

$$U_{ff\_th} = 5.7 - \frac{94.655}{U_{in}} . \quad (23)$$

From (23), the feedforward voltage U_{ff_th} is inversely proportional to the input voltage, so a divider should be used and cost will be increased. In order to reduce the cost and improve the accuracy, the approximate feedforward voltage (U_{ff_ap}) can be realized by two piecewise linear functions.

$$U_{ff\_ap} = \min \begin{cases} 0.166 U_{in} - 2.308 \\ 0.0585 U_{in} + 0.87 \end{cases} . \quad (24)$$

From (24), the voltage U_{ff_ap} is the smaller value in the two piecewise linear functions, which can be easily implemented by analog devices. Fig. 12 gives the implementation of U_{ff_ap}, where U_{rr} is the reference output voltage of SG3525, i.e., 5.1 V and U_{inf} is the feedback input voltage. Equations (23) and (24) can be plotted in Fig. 13. The error between (23) and (24) related to (23), i.e., $e\%$, is given in (25) and plotted in Fig. 13.

$$e\% = \frac{U_{ff\_ap} - U_{ff\_th}}{U_{ff\_th}} \times 100\% . \quad (25)$$

From Fig. 13, the error percentage $e\%$ is less than 5%, so the approximation accuracy is high.
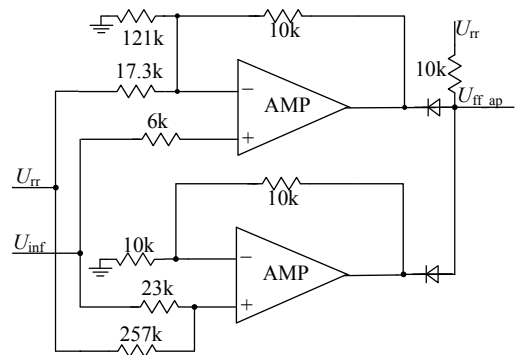

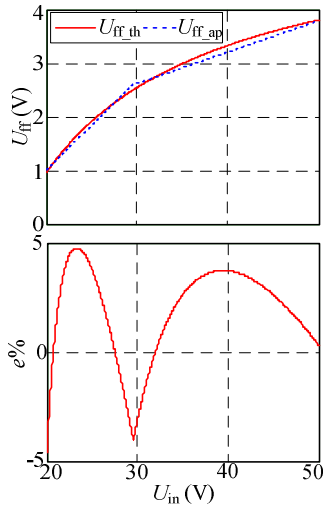Fig. 12. Implementation of linearization approximation.

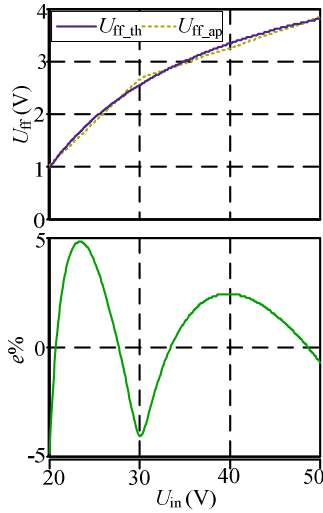Fig. 13. Chart of linearization approximation and error percentage.

Fig. 14. Simulation results of input voltage feedforward.

V. SIMULATION RESULTS

A 1-kW PPF TL converter is simulated to verify the theoretical analysis using the SABER software with the parameters given in Section IV. An ideal DC voltage source and an ideal resistive load are adopted in the simulation.

Fig. 14 shows the simulation results of input voltage feedforward. From Fig. 14, voltage U_{ff_ap} very approximates theoretical value U_{ff_th}. The error percentage is less than 5%. Therefore, simulation results verify the theoretical analysis.

Simulation results under startup is given in Fig. 15, where U_e is the reference voltage used to compare with the carrier voltage. As can be seen from Fig. 15, the proposed converter operates at current-limit control mode during startup, and the inductor current is limited to three times the rated output current. Therefore, the output voltage increases linearly. After the output voltage reaches the rated value, i.e., 380 V, the proposed converter operates at output-voltage control mode. After that, the system transfers to steady state gradually.
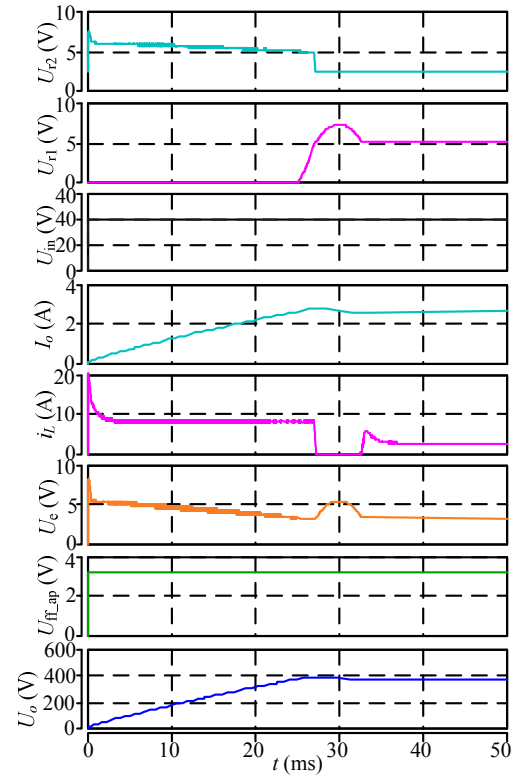

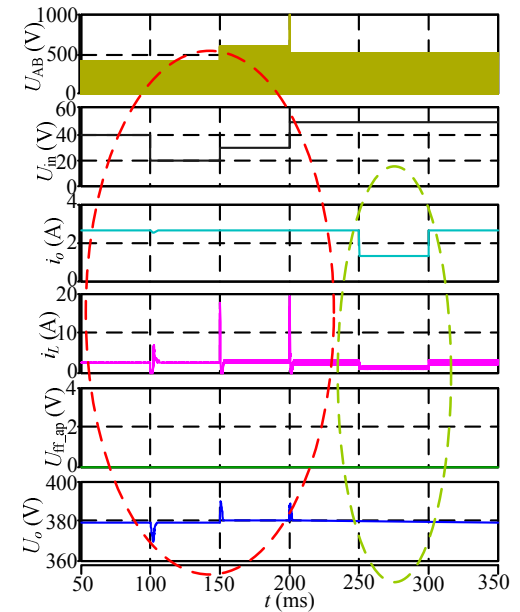
Fig. 15. Simulation results under startup.

Fig. 16. Simulation results under load and input voltage variations without input voltage feedforward.

Fig. 16 shows the simulation results under load and input voltage variations without input voltage feedforward. When the input voltage changes suddenly, current i_L has large inrush current and the output voltage is largely affected, shown in the left oval dashed line in Fig. 16. However, when the load changes from full to half loads and from half to full loads, the output voltage maintains constant, seen from the right oval dashed line in Fig. 16. When the input voltage changes from

30 V to 50 V, the maximum of U_{AB} is reduced. It means that three-level mode transfers to two-level mode. Therefore, the voltage stress of the rectifier diodes is reduced compared with the traditional two-level converter.

Fig. 17 gives the simulation results under load and input voltage variations with input voltage feedforward. As can be seen from Fig. 17, the feedforward voltage U_{ff_ap} changes with the input voltage, and current i_L is less affected and the output voltage keeps constant when input voltage changes, shown in the left oval dashed line in Fig. 17. Therefore, influences of input voltage on the output voltage and inductor current can be eliminated. When load current changes, the output voltage keeps constant, seen from the right oval dashed line in Fig. 17. Therefore, simulation results verify the theoretical analysis.
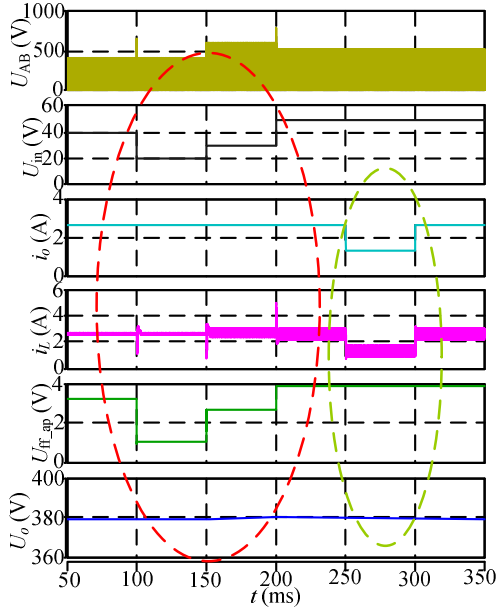

Fig. 17. Simulation results under load and input voltage variations with input voltage feedforward.

VI. Conclusions

This paper has proposed control and modeling of the PPF TL converter. The proposed converter can operate at both two-level and three-level modes, so it is suitable for wide input-voltage range application. Control degrees of freedom are the same as that in the traditional TL converter by adopting the proposed control method. Small-signal model of the proposed converter is established. Control block diagrams in both three-level and two-level modes are the same by maintaining the same gain of the modulator at both modes, so the control can be simplified, which is composed of output voltage loop, current limit loop, and input voltage feedforward. The output voltage loop is adopted to maintain the output voltage constant. The current limit loop is used to limit the output filter inductor current during startup or overload, while the input voltage feedforward is adopted to cancel the influences of input voltage on the output voltage and inductor current. The feedforward input voltage is approximated by two piecewise linear functions, which limit the error percent within 5%. Therefore, cost can be reduced since the divider is not needed. The concept also can be applied to other linearization approximation of the nonlinear function.

References

[1] N. Hatziargyriou, H. Asano, R. Iravani, and C. Marnay, "Microgrids," IEEE Power and Energy Magazine, vol. 5, no. 4, pp. 78–94, July/August 2007.

[2] M. Ehsani, Y. M. Gao, S. E. Gay, and A. Emadi, Modern Electric, Hybrid Electric, and Fuel Cell Vehicles Fundamentals, Theory, and Design. 2nd Edition, USA: CRC Press, 2004.

[3] Z. Yao and L. Xiao, "Push–pull forward three-level converter with reduced rectifier voltage stress," IEEE Transactions on Circuits and Systems–I: Regular Papers, vol. 57, no. 10, pp. 2815–2821, October 2010.

[4] X. Ruan, B. Li, Q. Chen, S.-C. Tan, and C.K. Tse, "Fundamental considerations of three-level DC–DC converters: topologies, analyses, and control," IEEE Transactions on Circuits and Systems I: Regular Papers, vol. 55, no. 11, pp. 3733–3743, November 2008.

[5] Z. Yao, G. Hu, and J. Kan, "Improved push-pull forward three-level converter," IEEE APPEEC, pp. 1–4, 2012.

[6] X. Ruan, Z. Chen, and W. Chen, "Zero-voltage-switching PWM hybrid full-bridge three-level converter," IEEE Transactions on Power Electronics, vol. 20, no. 2, pp. 395–404, March 2005.

[7] W. Chen and X. Ruan, "Zero-voltage-switching PWM hybrid full-bridge three-level converter with secondary-voltage clamping scheme," IEEE Transactions on Industrial Electronics, vol. 55, no. 2, pp. 644–654, February 2008.

[8] B. Arbetter and D. Maksimovic, "Feedforward pulse width modulators for switching power converters," IEEE Transactions on Power Electronics, vol. 12, no. 2, pp. 361–368, March 1997.

[9] P. Wu and J. Sun, "Control design optimization for an asymmetric half-bridge converter," IEEE COMPEL, pp. 1–8, 2010.

[10] X. Ruan, B. Li, Q. Chen, S.-C. Tan, and C.K. Tse, "Automatic mode-shifting control strategy with input voltage feed-forward for full-bridge-boost DC-DC converter suitable for wide input voltage range.," IEEE Transactions on Power Electronics, vol. 30, no. 3, pp. 1668–1682, March 2015.